Numerical dynamo simulations reproduce palaeomagnetic field behaviour

D. G. Meduri[1], A. J. Biggin[1], C. J. Davies[2], R. K. Bono[1], C. J. Sprain[3], J. Wicht[4]

[1]Department of Earth, Ocean and Ecological Sciences, University of Liverpool, Liverpool, UK
[2]School of Earth and Environment, University of Leeds, Leeds, UK
[3]Department of Geological Sciences, University of Florida, Gainesville, FL, USA
[4]Department Planets and Comets, Max Planck Institute for Solar System Research, Göttingen, Germany

Key Points:

- We present the first numerical geodynamo simulations known to reproduce the main features of palaeomagnetic field variability since 10 Ma
- All simulated characteristics of palaeomagnetic behaviour covary with the degree of dipole dominance (dipolarity)
- Only chemically driven dynamos at sufficiently low Ekman numbers in a specific dipolarity range capture palaeomagnetic field behaviour

Corresponding author: Domenico G. Meduri, `domenico.meduri@liverpool.ac.uk`

Abstract

Numerical geodynamo simulations capture several features of the spatial and temporal geomagnetic field variability on historical and Holocene timescales. However, a recent analysis questioned the ability of these numerical models to comply with long-term palaeomagnetic field behaviour. Analysing a suite of 50 geodynamo models, we present here the first numerical simulations known to reproduce the salient aspects of the palaeosecular variation and time-averaged field behaviour since 10 Ma. We find that the simulated field characteristics covary with the relative dipole field strength at the core-mantle boundary (dipolarity). Only models dominantly driven by compositional convection, with an Ekman number (ratio of viscous to Coriolis forces) lower than 10^{-3} and a dipolarity in the range $0.34-0.56$ can capture the observed palaeomagnetic field behaviour. This dipolarity range agrees well with state-of-the-art statistical field models and represent a testable prediction for next generation global palaeomagnetic field model reconstructions.

Plain Language Summary

Earth's magnetic field varies on a wide range of timescales, from less than a year to hundreds of million years or longer. Such variations are produced by the complex fluid dynamic processes in the liquid iron core, which are generally studied using 3D computer simulations. While these simulations reproduce several features of the geomagnetic field on relatively short timescales (less than 10 kyr), their compliance with the field characteristics on longer timescales has been recently questioned. Here we present the first simulations known to reproduce the salient features of the geomagnetic magnetic field behaviour over the last 10 Myr. Analysing a large suite of simulations, we demonstrate that the most Earth-like ones employ buoyancy sources modelling the release of light elements from the inner core, have a low enough viscosity and a magnetic field morphology which is sufficiently, but not too strongly, dipolar. Our estimates of the degree of dipole dominance agree well with those obtained from observational field models. Our findings can be employed by future studies to reliably simulate long-term geomagnetic field behaviour, hence improving our understanding of the Earth's core and its evolution.

1 Introduction

The geomagnetic field varies on a striking range of spatial and temporal scales. These variations can be characterised through direct observations only for the last four centuries, while on longer timescales information is available indirectly through palaeomagnetic and archaeomagnetic measurements. By tying together observations and numerical simulations of the dynamo process in the outer core, we can gain fundamental insights into the physics of the deep interior through geologic time.

Numerical dynamo simulations reproduced several features of the geomagnetic field, including a dipole-dominated field and polarity reversals (see, e.g., Christensen & Wicht, 2015), the fundamental time-averaged morphological properties of the historical field (Christensen et al., 2010), and the axial dipole variations observed over Holocene timescales (Davies & Constable, 2014). However, due to the current computational limitations, geodynamo simulations cannot run at the extreme conditions that characterise the turbulent core fluid. Such limitations are particularly severe when studying the long-term field behaviour, since long time integrations are needed. Recently, Sprain et al. (2019) (S19 hereafter) raised the question of how Earth-like was the long-term field behaviour displayed by dynamo simulations. Defining a set of criteria ($Q_{\rm PM}$ criteria) to quantify the degree of semblance of geodynamo simulations with the palaeomagnetic field of the last 10 Myr, the authors found that none of the 46 simulations explored could capture the main aspects of the observed variability. In fact, the large majority of the simulations performed poorly; only a few passed three out of the five $Q_{\rm PM}$ criteria with large total misfits.

Here we present a new set of simulations reproducing palaeomagnetic field behaviour of the last 10 Myr according to the Q_{PM} criteria. First, we show that the relative strength of the dipole field to the total field up to spherical harmonic degree and order 12 at the core-mantle boundary (CMB) can be used as a proxy for all palaeomagnetic observables considered. We then examine the conditions for obtaining palaeomagnetic-like simulations and discuss implications for the Earth's core.

2 Methods

2.1 Model Formulation

The setup and solution method for the geodynamo models are standard and extensively documented elsewhere (Willis et al., 2007; Davies & Constable, 2014; Wicht, 2002; Wicht & Meduri, 2016, WM16 hereafter). We therefore provide only a brief description here (see also Section S1). We consider a convection-driven magnetohydrodynamic flow under the Boussinesq approximation with the fluid confined to a spherical shell of thickness $d = r_{\mathrm{o}} - r_{\mathrm{i}}$ rotating at a constant angular velocity Ω. Here r_{i} and r_{o} are the inner and outer boundary radii, which are identified with the inner core radius and the CMB radius, respectively.

All models assume no-slip mechanical boundary conditions and an electrically insulating mantle. We employ the codensity approach where density perturbations due to compositional and temperature differences are described by only one variable. Different convective driving scenarios are modelled via the boundary conditions and homogeneous volumetric codensity sinks. Thermal dynamos are bottom heated with either fixed flux or fixed temperature at r_{i}. All the heat entering at r_{i} leaves the system through r_{o} where a fixed flux condition is imposed. Some models employ lateral variations in the outer boundary heat flux in the form of a recumbent spherical harmonic (SH) of degree $\ell = 2$ and order $m = 0$ as an approximation of the observed lower mantle seismic shear-wave structures (Dziewonski et al., 2010).

Chemical dynamos are driven by either a fixed light element concentration or concentration gradient at r_{i}, which is balanced by a volumetric sink. The flux through r_{o} is set to zero. While the chemical dynamos assume an electrically conducting inner core, the thermal dynamos use an insulating inner core for simplicity. Wicht (2002) showed that the impact of inner core conductivity on the magnetic field and its variability is minor in thermal dynamos, although this may depend on the details of the convective driving and mechanical boundary conditions employed (Dharmaraj & Stanley, 2012; Lhuillier et al., 2013).

The dimensionless parameters controlling the system are the Ekman number Ek, the Prandtl number Pr, the magnetic Prandtl number Pm and the shell aspect ratio χ:

$$\mathrm{Ek} = \frac{\nu}{\Omega d^2}, \quad \mathrm{Pr} = \frac{\nu}{\kappa} = 1, \quad \mathrm{Pm} = \frac{\nu}{\eta}, \quad \chi = \frac{r_{\mathrm{i}}}{r_{\mathrm{o}}} = 0.35. \tag{1}$$

Here ν, η and κ are the kinematic viscosity, magnetic diffusivity and thermal (or compositional) diffusivity of the fluid, respectively. The Rayleigh number controls the vigour of convection and is defined in Section S1. Ek varies between 3×10^{-4} and 2×10^{-3}, and Pm spans the range $3 - 10$. These ranges are constrained by the need to perform long temporal integrations.

Our dataset is summarised in Table S1 and consists of 50 simulations: 21 from S19, 7 from WM16 and 22 are new runs. From S19 we excluded thermal dynamos which use specific buoyancy profiles (Davies & Gubbins, 2011), large amplitudes of the CMB heat flux anomalies ($\epsilon = 1.5$; see Table S1 for the definition of ϵ), and low Rayleigh numbers (regime of locked dynamo action). We also excluded the cases at $\mathrm{Pm} = 20$. All these simulations poorly comply with Earth having total Q_{PM} misfits larger than 5 and total Q_{PM} scores of 3 at most (see Section 2.2). The new thermal runs complement the Rayleigh number range explored by S19 and include cases at $\mathrm{Ek} = 3\times10^{-4}$. The new chemical runs are similar to those of WM16 but focus on reversing dipolar solutions.

2.2 Palaeomagnetic Criteria for Geodynamo Simulations

The Q_{PM} framework is described in detail in S19 and we recall only the essentials here. S19 identified five palaeomagnetic observables that describe the long-term palaeosecular variation (PSV) and time-averaged field (TAF) behaviour. The first two observables characterise the virtual geomagnetic pole (VGP) angular dispersion S by estimating its equatorial value and latitudinal dependence. They are the parameters a and b of the empirical quadratic fit with palaeolatitude λ introduced by McFadden et al. (1988),

$$S^2 = a^2 + (b\lambda)^2. \tag{2}$$

The third Q_{PM} observable is the absolute maximum of the inclination anomaly

$$\Delta I = \bar{I} - I_{GAD}, \tag{3}$$

which is function of latitude. Here $\bar{I}$ is the Fisher mean inclination (Fisher, 1953) and I_{GAD} is the inclination expected under a geocentric axial dipole field. The fourth observable, $V\%$, is the ratio of the interquartile range to the median of the virtual dipole moment (VDM) distribution. The last observable is the relative transitional time τ_{T}, defined as the fraction of time spent with an absolute true dipole latitude lower than $45°$, which is complemented with a criterion on the presence of reversals.

Using the most recent compilation of palaeomagnetic directional data PSV10 (Cromwell et al., 2018) and the palaeointensity database PINT (Biggin et al., 2009, 2015), S19 estimated values and uncertainties of these five observables for the last 10 Myr (see Table S2). The sum of normalised linear misfits between simulated and observed values for each Q_{PM} observable is ΔQ_{PM}. If the normalised misfit of a given observable is ≤ 1, the observed and simulated palaeomagnetic characteristics overlap within the respective estimated uncertainties.

Together with the misfits, S19 defined binary scores. The score of a given Q_{PM} observable is 1 if the normalised misfit in that observable is ≤ 1 and is zero otherwise. The total score Q_{PM}, obtained by summing the single scores, thus ranges from 0 to 5. By definition, a palaeomagnetic-like simulation with the maximum score $Q_{\mathrm{PM}} = 5$ has a total misfit $\Delta Q_{\mathrm{PM}} \leq 5$. Even when $Q_{\mathrm{PM}} < 5$, however, the total misfit can be smaller than 5. While a large Q_{PM} signifies a good compliance with Earth, a large ΔQ_{PM} means the opposite.

3 Results

3.1 Evidence for Palaeomagnetic-Like Geodynamo Simulations

The magnetic fields obtained in geodynamo simulations are generally characterised by their degree of dipole dominance, which is often measured by the dipolarity D_{12}, defined as the time-averaged ratio of the root mean square (RMS) dipole field strength to the total RMS field strength up to SH degree and order $\ell = m = 12$ at the CMB (Christensen & Aubert, 2006). Multipolar solutions generally have $D_{12} \lesssim 0.35$, while dominantly dipolar ones like the present geomagnetic field have $D_{12} \gtrsim 0.7$ (Christensen & Aubert, 2006; Christensen, 2010). Dipolar reversing solutions, that is dynamos which are dipole dominated most of the time but occasionally undergo polarity reversals, occur in a narrow dipolarity range sandwiched between the stable dipolar and the multipolar regimes (Driscoll & Olson, 2009; Wicht & Tilgner, 2010; Wicht et al., 2015).

Figure 1a,b demonstrates that D_{12} is a good proxy for the total misfit ΔQ_{PM}. When the Rayleigh number increases (in the direction indicated by the arrows in the connected

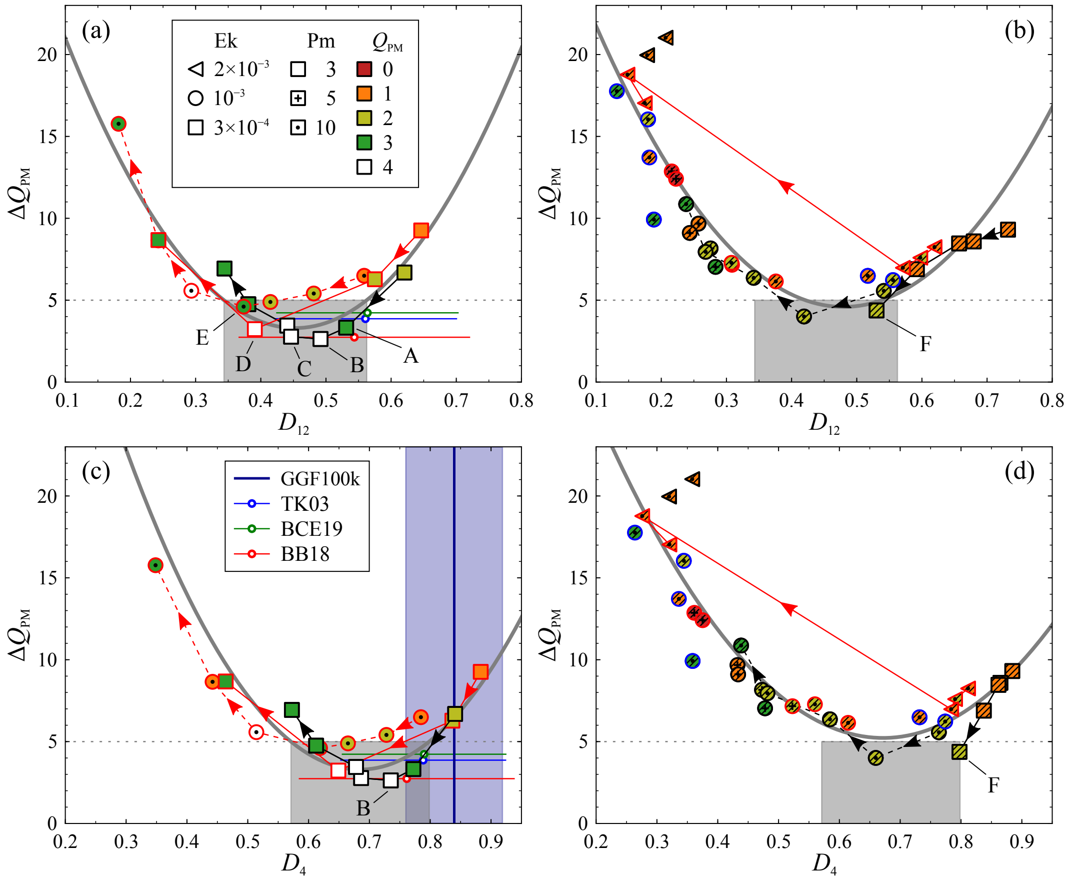

Figure 1. (a,b) Total misfit $\Delta Q_{\rm PM}$ as a function of the dipolarity D_{12} for the (a) chemical and (b) thermal (hatched symbols hereafter) runs. The symbol shape and colour code Ek and the total score $Q_{\rm PM}$ respectively; the marker inside the main symbol indicates Pm (see the legend inset in (a)). The symbol rim colour denotes the codensity boundary conditions (black: fixed heat/compositional flux at $r_{\rm i}$; red: fixed temperature/composition at $r_{\rm i}$; blue: presence of lateral heat flux variations at $r_{\rm o}$). Connecting lines show simulations differing only in the Rayleigh number, which increases in the direction indicated by the arrows (for clarity, only three tracks are presented in (b)). The grey curves are quadratic fits to the chemical runs at Ek $= 3 \times 10^{-4}$ and to all thermal runs. Palaeomagnetic-like simulations are found in the grey shaded region of horizontal extent δD_{12} which is defined by the chemical runs as explained in the main text. (c,d) Same as (a) and (b) but for the modified dipolarity D_4. The vertical blue line in (c) shows the palaeomagnetic field model GGF100k of Panovska et al. (2018) (the shaded region displays one standard deviation above and below D_4). Circles with error bars in (a) and (c) present the GGP models TK03 (Tauxe & Kent, 2004), BCE19 (Brandt et al., 2020) and BB18 (Bono et al., 2020) (error bars denote one standard deviation above and below the dipolarity values). Capital letters A–F mark the six simulation runs discussed in the main text (see Table S1 for additional information).

lines in Figure 1) the dipolarity systematically decreases together with ΔQ_{PM} until $D_{12} \approx 0.5$. For smaller values of D_{12}, ΔQ_{PM} increases again and the simulations roughly describe parabolic paths in the D_{12}-ΔQ_{PM} plane. These paths show no apparent dependence on the codensity boundary conditions or on Pm (see also Figure S1), but depend strongly on the convective driving mode and on the Ekman number. While the thermal dynamos barely reach misfits of $\Delta Q_{\mathrm{PM}} \approx 4$ with a score $Q_{\mathrm{PM}} = 2$ (Figure 1b), the chemical runs show ΔQ_{PM} as low as 2.7 with $Q_{\mathrm{PM}} = 4$ (Figure 1a). In fact, these latter runs come close to a score of $Q_{\mathrm{PM}} = 5$, having either a moderately low relative transitional time or an equatorial dispersion only a few degrees higher than Earth (Section 3.2.1). These palaeomagnetic-like dynamos combine chemical driving with the lower $\mathrm{Ek} = 3\times 10^{-4}$. The chemical runs at $\mathrm{Ek} = 10^{-3}$ barely reach $\Delta Q_{\mathrm{PM}} \approx 5$ with $Q_{\mathrm{PM}} = 3$.

Remarkably, the optimal field solutions, i.e. those which yield the lowest ΔQ_{PM} and the highest Q_{PM} in each Rayleigh number track, lie in a well defined D_{12} range. The quadratic function $\Delta Q_{\mathrm{PM}} = c_0 + c_1 D_{12} + c_2 (D_{12})^2$ well describes the simulation behaviour in both types of convective forcing with a high coefficient of determination R^2 (grey curves in Figure 1a,b; see Table S3 for values of the regression coefficients and R^2). The minima of the quadratic fits occur at $D_{12} = 0.45$ and $D_{12} = 0.48$ for the chemical and thermal runs respectively. Small departures from these values cause a large increase of ΔQ_{PM} and a decrease in Q_{PM}. The values of D_{12} where the quadratic fit of the chemical runs at $\mathrm{Ek} = 3\times 10^{-4}$ intersects the threshold $\Delta Q_{\mathrm{PM}} = 5$ below which Earth-like models are expected define the dipolarity interval $\delta D_{12} = [0.34, 0.56]$.

The dipolarity values of our palaeomagnetic-like dynamos are compatible with estimates obtained for Earth from global palaeomagnetic field model reconstructions. Since these models have spatial power spectra that are generally considered to be well resolved only for SH degrees $\ell \leq 4$ (Korte & Constable, 2008; Wardinski & Korte, 2008; Nilsson et al., 2014, see also Figure S2), we analyse the modified dipolarity D_4 which includes SH contributions up to $\ell = m = 4$. Note, however, that even degrees $\ell \leq 4$ may suffer from spatial and temporal regularisations (Sanchez et al., 2016; Hellio & Gillet, 2018) and the true D_4 values may be somewhat smaller. Figure 1c,d shows that the behaviour of D_4 can also be described by a simple quadratic dependence. The palaeomagnetic-like dipolarity interval predicted by our chemical dynamos at $\mathrm{Ek} = 3\times 10^{-4}$ is $\delta D_4 = [0.57, 0.80]$.

GGF100k (Panovska et al., 2018), the longest global field reconstruction to date, spans the last 100 kyr and provides $D_4 = 0.84 \pm 0.08$, in relatively good agreement with our numerical prediction (Figure 1c; see also Table S4). LSMOD.2 (Brown et al., 2018) has a lower value of $D_4 = 0.74$ since it deliberately models the field during the two most recent excursions. This lower estimate falls within δD_4 and is in excellent agreement with the value obtained for run B, our most palaeomagnetic-like simulation (Figure 1c and Table S4).

For field reconstructions covering shorter time intervals, the Holocene CALS10k.1b (Korte et al., 2011) model provides $D_4 = 0.92$, and the historical gufm1 (Jackson et al., 2000) and IGRF-13 (Thébault et al., 2015) models give $D_4 = 0.88$ and 0.82 respectively. Such high values of D_4 are likely due to the short timespans sampled by these models. It is encouraging that the differences with our numerical predictions of D_4 reduce for the longer time averages obtained from GGF100k and LSMOD.2.

Estimates of D_{12} for Earth on timescales of million years can be obtained from statistical field models based on a giant Gaussian process (GGP). Here we consider the GGP models TK03 (Tauxe & Kent, 2004), BCE19 (Brandt et al., 2020) and BB18 (Bono et al., 2020), which are explicitly constructed to reproduce the PSV over the last $5-10$ Myr, with BB18 also capturing the observed VDM distribution. TK03 and BCE19 differ only in the assumed variances of their independent and normally distributed Gauss coefficients, while BB18 additionally employs a covariance pattern for degrees $\ell \leq 4$ inferred from dynamo simulations. These GGP models have $0.54 \leq D_{12} \leq 0.56$ and thus fall within the palaeomagnetic-like interval δD_{12} predicted here (see Figure 1a and also Table S4).

3.2 Description of the Simulated Long-Term Field Behaviour

3.2.1 Variation of the Palaeomagnetic Observables With D_{12}

Figure 2 presents the five $Q_{\rm PM}$ observables as a function of D_{12} for all chemical runs. All observables increase as D_{12} decreases, a trend which is also observed for the thermal dynamos (Figure S3). Though our three most palaeomagnetic-like simulations (runs B–D) only reach a total score of 4 (Figure 1a), they still reproduce the single missed $Q_{\rm PM}$ observable to a reasonable level.

Run B closely captures all observables except the relative transitional time $\tau_{\rm T}$ (Figure 2; Table S4), which is too small at 0.018, about half the Earth's lower bound value (Table S2). While this run showed one reversal and three excursions in 35 magnetic diffusion times, we cannot exclude it may yield Earth-like $\tau_{\rm T}$ when a robust statistic is obtained for longer integrations. Runs C and D have Earth-like transitional times ($\tau_{\rm T} =$ 0.046 and 0.065 respectively; Figure 2e) but a median equatorial dispersion a about 4° and 6° too high with misfits < 1.6 (Figure 2a; Tables S2 and S4). Relaxing the uncertainties on a by $< 2°$ would yield a total score of 5 for these two runs. On this basis, we consider the simulated palaeomagnetic behaviour of runs B–D to be an excellent approximation to that of Earth in the last 10 Myr, while acknowledging it does not quite meet the full requirements for being classified as "Earth-like" by the current $Q_{\rm PM}$ criteria.

3.2.2 Influence of the Ekman Number in Chemical Dynamos

As well as intermediate values of D_{12}, chemical dynamos can reach low misfits and high scores only if the Ekman number is low enough (Section 3.1). This dependency on Ek results from the behaviour of a and $\tau_{\rm T}$. In the palaeomagnetic-like dipolarity interval δD_{12}, chemical dynamos at $\mathrm{Ek} = 10^{-3}$ have comparable or higher a and lower $\tau_{\rm T}$ than the cases at $\mathrm{Ek} = 3\times10^{-4}$ (Figure 2a,e). Misfits in a and $\tau_{\rm T}$ are up to three times smaller in these low-Ek runs compared to the high-Ek cases, while misfits in the other $Q_{\rm PM}$ observables are similar (for example, in Table S4 compare run D with run E, the simulation with the lowest $\Delta Q_{\rm PM}$ at $\mathrm{Ek} = 10^{-3}$).

In the simulations at $\mathrm{Ek} = 10^{-3}$, more frequent polarity transitions leading to Earth-like values of $\tau_{\rm T}$ start at $D_{12} \approx 0.3$ where a is already far too high (Figure 3a; white symbols show Earth-like $\tau_{\rm T}$). At the lower Ek of 3×10^{-4}, on the other hand, reversals start to appear at $D_{12} \approx 0.45$ where a is still relatively Earth-like. Such a dependency on Ek for the onset of reversals arises because the dipole field variability, measured by the relative standard deviation $\sigma_{\rm d}/\overline{B}_{\rm d}$ (the ratio of the standard deviation of the dipole field strength at the CMB to its time-averaged value), increases with decreasing Ek in our simulations (Figure 3b). These larger dipole fluctuations naturally lead to an increased likelihood of both transitional periods and polarity reversals (Driscoll & Olson, 2009; Meduri & Wicht, 2016, WM16). We note that a remains Earth-like in the low-Ek runs at $D_{12} \gtrsim$ 0.45 since the equatorially symmetric CMB field, which determines a (McFadden et al., 1988; Coe & Glatzmaier, 2006), is weaker than in the high-Ek cases in the same dipolarity range (Figure S4).

3.2.3 Influence of the Convective Driving Mode

Thermal dynamos at $\mathrm{Ek} = 3\times10^{-4}$ do not reach $\Delta Q_{\rm PM}$ as low and $Q_{\rm PM}$ as high as the chemical dynamos at the same Ekman number (Section 3.1). In these runs, the $Q_{\rm PM}$ observables vary similarly with D_{12}, with the exception of the latitudinal VGP dis-

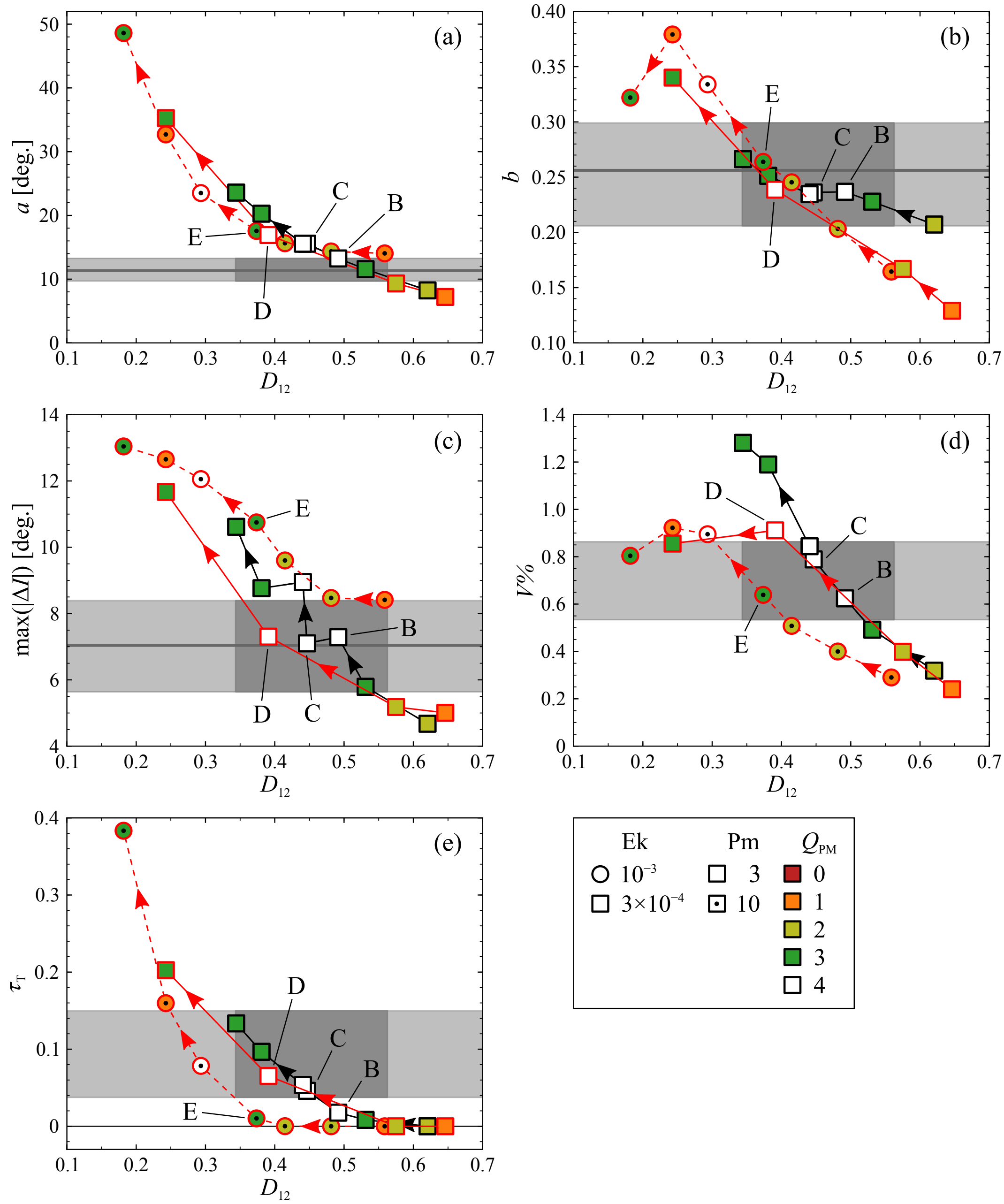

Figure 2. $Q_{\rm PM}$ observables as a function of the dipolarity D_{12} for all chemical runs. For the meaning of the symbols and connecting lines, see the legend at the bottom right and Figure 1. The horizontal grey regions show Earth's $Q_{\rm PM}$ observables (solid lines denote median values; shading displays the estimated 95% confidence intervals or the assumed bounds; see Table S2 for further details). Dark grey shaded regions highlight the predicted palaeomagnetic-like dipolarity interval δD_{12}.

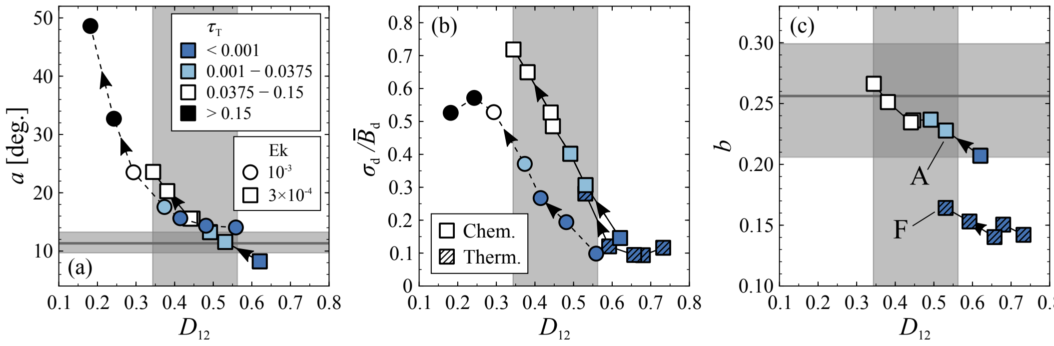

Figure 3. (a) Equatorial VGP dispersion a, (b) relative standard deviation of the CMB dipole field strength $\sigma_d/\overline{B}_d$ and (c) latitudinal VGP dispersion b as a function of the dipolarity D_{12} for selected Rayleigh number tracks (chemical runs are those at $\mathrm{Ek} = 10^{-3}$ and at $\mathrm{Ek} = 3 \times 10^{-4}$ with fixed inner boundary flux in Figures 1a and 2; thermal runs are those at $\mathrm{Ek} = 3 \times 10^{-4}$ in Figures 1b and S3). The symbol colour codes the relative transitional time τ_T as indicated in the legend inset in (a) (Earth-like τ_T according to Q_{PM} criteria in white). The horizontal grey regions in (a) and (c) show Earth's a and b values as in Figure 2a,b. The vertical grey region displays the predicted palaeomagnetic-like dipolarity interval δD_{12}.

persion b and τ_T (Figure S3). The thermal runs, unlike the chemical ones, present values of b which remain low and non-Earth-like for all D_{12} explored (Figure 3c). The weak variation of b with D_{12} in the thermal runs can be attributed to the almost unchanged odd and even CMB field contributions (Figure S4). The chemical runs, unlike the thermal cases, already show reversals at an intermediate D_{12}. At $D_{12} = 0.53$, for example, run F (thermal) shows a stable dipolar solution with $\tau_T = 0$, whereas run A (chemical) undergoes few excursions so that $\tau_T = 0.01$ (Figure 3c; see also Figure S3e). Chemical dynamos then reach Earth-like τ_T at slightly lower values of D_{12} where also the other Q_{PM} observables are captured.

4 Discussion and Conclusions

We tested whether a new set of numerical dynamo simulations reproduces the palaeomagnetic field behaviour of the last 10 Myr by applying the Q_{PM} criteria of S19. These criteria examine the equatorial and latitudinal VGP dispersion, the inclination anomaly, the VDM distribution, and the relative time spent by the true dipole pole in transitional latitudes, along with the presence of reversals.

We reported the first numerical simulations known to reproduce these fundamental characteristics of the palaeomagnetic field since 10 Ma. The dipolarity D_{12}, which measures the degree of dipole dominance at the CMB, appears to be a good proxy for all five Q_{PM} observables across a variety of simulations differing in control parameters, boundary conditions and convective driving mode, and it allows predictions of the total Q_{PM} misfit and score. Simulations capturing the observed field behaviour are characterised by (i) a compositional driving, (ii) an Ekman number Ek below 10^{-3} and (iii) a dipolarity D_{12} in the interval $\delta D_{12} = [0.34, 0.56]$. Previous numerical studies exploring long-term geomagnetic field behaviour do not generally employ simulations that fulfil all such conditions; for example, they often use $\mathrm{Ek} \gtrsim 10^{-3}$ due to computational reasons.

Our best performing simulations employ a setup where buoyancy is released at the inner core boundary and absorbed by the outer core. This seems an appropriate scenario for the geodynamo after the inner core started crystallising and the light elements, emanated from the growing inner core front, may have dominated convective driving (Nimmo, 2015; Labrosse, 2015). Taken at face value, our analysis appears to favour compositional over thermal convection as the dominant driving mode of the geodynamo over the last 10 Myr, in agreement with both thermal history calculations (see, e.g., Nimmo, 2015) and numerical dynamo studies exploring the influence of the two convective drivings on the magnetic field morphology (Kutzner & Christensen, 2000).

The dipolarity interval δD_{12} where palaeomagnetic-like simulations are found is bounded above by the modern field. Current GGP models provide an estimate of D_{12} for Earth of about 0.55, which falls within δD_{12} and confirms the robustness of our numerical results. The suggested dipolarity interval represents a specific, testable prediction for next generation palaeomagnetic field models, once they reach higher spatial resolutions and cover longer time intervals than the models currently available. Earth's core may lie at the transition between the dipolar and the multipolar dynamo regimes (Christensen & Aubert, 2006; Oruba & Dormy, 2014) and our results are compatible with this finding. This transition indeed occurs at D_{12} in the range $0.35-0.50$, which is included in the palaeomagnetic-like interval δD_{12} predicted here.

Our results suggest the possibility of constructing a path towards Earth's core conditions which preserves palaeomagnetic-like dynamo characteristics. According to Oruba and Dormy (2014), the parameter combination $\mathrm{Re}\,\mathrm{Ek}^{2/3}$ ($\mathrm{Re} = \mathrm{U}d/\nu$ is the Reynolds number, where U is the time-averaged RMS core flow velocity) defines the dipolar-multipolar transition at $D_{12} \approx 0.5$, which is close to the optimal value $D_{12} = 0.45$ inferred from our analysis. To maintain D_{12} constant while reducing Ek, Re needs to increase and this can be achieved by increasing the Rayleigh number and by decreasing Pm. Following this path to lower Ek and Pm and higher Rayleigh numbers, the relevant balance for the Earth's core between magnetic, Coriolis and buoyancy forces is expected to emerge naturally, as also suggested by recent high-resolution numerical simulations (Yadav et al., 2016; Schaeffer et al., 2017; Aubert et al., 2017; Aubert, 2019).

It has recently been argued that the geomagnetic field displayed similar average degrees of surface axial dipole dominance over large swathes of geological time (Biggin et al., 2020). Insofar as dipolarity and surface axial dipole dominance may be assumed to be related, we expect that many of the conclusions reached here are also valid at certain earlier times in Earth's history.

Acknowledgments

Funding for DGM, AJB and RKB was provided by The Leverhulme Trust Research Leadership Award, RL-2016-080; for CJD, by the NERC fellowship NE/L011328/1. AJB and CJS additionally acknowledge funding from NERC Standard Grant NE/P00170X/1. The authors declare no competing financial interests. A portion of the geodynamo simulations were performed on the UK National Supercomputing Service ARCHER and on ARC, part of the High Performance Computing facilities at the University of Leeds, UK. The authors thank the two anonymous reviewers and are grateful to Richard Holme for helpful discussions. The simulation output data used to produce Figures 1–3 can be found in the supplementary information and can be accessed via DOI 10.17605/OSF.IO/PY85T.

References

Aubert, J. (2019). Approaching Earth's core conditions in high-resolution geodynamo simulations. *Geophysical Journal International*, *219*(Supplement 1), S137–S151. doi: 10.1093/gji/ggz232

Aubert, J., Gastine, T., & Fournier, A. (2017). Spherical convective dynamos in the rapidly rotating asymptotic regime. *Journal of Fluid Mechanics*, *813*, 558–593.

doi: 10.1017/jfm.2016.789

Biggin, A. J., Bono, R. K., Meduri, D. G., Sprain, C. J., Davies, C. J., Holme, R., & Doubrovine, P. V. (2020). Quantitative estimates of average geomagnetic axial dipole dominance in deep geological time. *Nature Communications*, *11*, 6100. doi: 10.1038/s41467-020-19794-7

Biggin, A. J., Piispa, E. J., Pesonen, L. J., Holme, R., Paterson, G. A., Veikkolainen, T., & Tauxe, L. (2015). Palaeomagnetic field intensity variations suggest mesoproterozoic inner-core nucleation. *Nature*, *526*, 245–248. doi: 10.1038/nature15523

Biggin, A. J., Strik, G. H. M. A., & Langereis, C. G. (2009). The intensity of the geomagnetic field in the late-archaean: new measurements and an analysis of the updated iaga palaeointensity database. *Earth, Planets and Space*, *61*, 9–22. doi: 10.1186/BF03352881

Bono, R. K., Biggin, A. J., Holme, R., Davies, C. J., Meduri, D. G., & Bestard, J. (2020). Covariant giant gaussian process models with improved reproduction of palaeosecular variation. *Geochemistry, Geophysics, Geosystems*, *21*(8), e2020GC008960. doi: 10.1029/2020GC008960

Brandt, D., Constable, C., & Ernesto, M. (2020). Giant Gaussian process models of geomagnetic palaeosecular variation: a directional outlook. *Geophysical Journal International*, *222*(3), 1526–1541. doi: 10.1093/gji/ggaa258

Brown, M., Korte, M., Holme, R., Wardinski, I., & Gunnarson, S. (2018). Earth's magnetic field is probably not reversing. *Proceedings of the National Academy of Sciences*, *115*(20), 5111–5116. doi: 10.1073/pnas.1722110115

Christensen, U., & Wicht, J. (2015). 8.10 - Numerical dynamo simulations. In G. Schubert (Ed.), *Treatise on geophysics (second edition)* (Second Edition ed., pp. 245–277). Oxford: Elsevier. doi: 10.1016/B978-0-444-53802-4.00145-7

Christensen, U. R. (2010). Dynamo Scaling Laws and Applications to the Planets. *Space Science Review*, *152*(1–4), 565–590. doi: 10.1007/s11214-009-9553-2

Christensen, U. R., & Aubert, J. (2006). Scaling properties of convection-driven dynamos in rotating spherical shells and application to planetary magnetic fields. *Geophysical Journal International*, *166*(1), 97–114. doi: 10.1111/j.1365-246X.2006.03009.x

Christensen, U. R., Aubert, J., & Hulot, G. (2010). Conditions for Earth-like geodynamo models. *Earth and Planetary Science Letters*, *296*(3), 487–496. doi: 10.1016/j.epsl.2010.06.009

Coe, R. S., & Glatzmaier, G. A. (2006). Symmetry and stability of the geomagnetic field. *Geophysical Research Letters*, *33*(21). doi: 10.1029/2006GL027903

Cromwell, G., Johnson, C. L., Tauxe, L., Constable, C. G., & Jarboe, N. A. (2018). Psv10: A global data set for 0–10 ma time-averaged field and paleosecular variation studies. *Geochemistry, Geophysics, Geosystems*, *19*(5), 1533–1558. doi: 10.1002/2017GC007318

Davies, C. J., & Constable, C. G. (2014). Insights from geodynamo simulations into long-term geomagnetic field behaviour. *Earth and Planetary Science Letters*, *404*, 238–249. doi: 10.1016/j.epsl.2014.07.042

Davies, C. J., & Gubbins, D. (2011). A buoyancy profile for the Earth's core. *Geophysical Journal International*, *187*(2), 549–563. doi: 10.1111/j.1365-246X.2011.05144.x

Dharmaraj, G., & Stanley, S. (2012). Effect of inner core conductivity on planetary dynamo models. *Physics of the Earth and Planetary Interiors*, *212–213*, 1–9. doi: 10.1016/j.pepi.2012.09.003

Driscoll, P., & Olson, P. (2009). Effects of buoyancy and rotation on the polarity reversal frequency of gravitationally driven numerical dynamos. *Geophysical Journal International*, *178*(3), 1337–1350. doi: 10.1111/j.1365-246X.2009.04234.x

Dziewonski, A. M., Lekic, V., & Romanowicz, B. A. (2010). Mantle anchor structure: An argument for bottom up tectonics. *Earth and Planetary Science Letters*, *299*(1), 69–79. doi: 10.1016/j.epsl.2010.08.013

Fisher, R. A. (1953). Dispersion on a sphere. *Proceedings of the Royal Society of London. Series A. Mathematical and Physical Sciences*, *217*(1130), 295–305. doi: 10.1098/rspa.1953.0064

Hellio, G., & Gillet, N. (2018). Time-correlation-based regression of the geomagnetic field from archeological and sediment records. *Geophysical Journal International*, *214*(3), 1585–1607. doi: 10.1093/gji/ggy214

Jackson, A., Jonkers, A. R. T., & Walker, M. R. (2000). Four centuries of geomagnetic secular variation from historical records. *Philosophical Transactions of the Royal Society of London. Series A: Mathematical, Physical and Engineering Sciences*, *358*(1768), 957–990. doi: 10.1098/rsta.2000.0569

Korte, M., & Constable, C. (2008). Spatial and temporal resolution of millennial scale geomagnetic field models. *Advances in Space Research*, *41*(1), 57 - 69. doi: 10.1016/j.asr.2007.03.094

Korte, M., Constable, C., Donadini, F., & Holme, R. (2011). Reconstructing the holocene geomagnetic field. *Earth and Planetary Science Letters*, *312*(3), 497–505. doi: 10.1016/j.epsl.2011.10.031

Kutzner, C., & Christensen, U. (2000). Effects of driving mechanisms in geodynamo models. *Geophysical Research Letters*, *27*(1), 29–32. doi: 10.1029/1999GL010937

Labrosse, S. (2015). Thermal evolution of the core with a high thermal conductivity. *Physics of the Earth and Planetary Interiors*, *247*, 36–55. doi: 10.1016/j.pepi.2015.02.002

Lhuillier, F., Hulot, G., & Gallet, Y. (2013). Statistical properties of reversals and chrons in numerical dynamos and implications for the geodynamo. *Physics of the Earth and Planetary Interiors*, *220*, 19–36. doi: 10.1016/j.pepi.2013.04.005

McFadden, P. L., Merrill, R. T., & McElhinny, M. W. (1988). Dipole/quadrupole family modeling of paleosecular variation. *Journal of Geophysical Research: Solid Earth*, *93*(B10), 11583–11588. doi: 10.1029/JB093iB10p11583

Meduri, D. G., & Wicht, J. (2016). A simple stochastic model for dipole moment fluctuations in numerical dynamo simulations. *Frontiers in Earth Science*, *4*, 38. doi: 10.3389/feart.2016.00038

Nilsson, A., Holme, R., Korte, M., Suttie, N., & Hill, M. (2014). Reconstructing Holocene geomagnetic field variation: new methods, models and implications. *Geophysical Journal International*, *198*(1), 229–248. doi: 10.1093/gji/ggu120

Nimmo, F. (2015). 8.02 - Energetics of the core. In G. Schubert (Ed.), *Treatise on geophysics (second edition)* (Second Edition ed., pp. 27–55). Oxford: Elsevier. doi: 10.1016/B978-0-444-53802-4.00139-1

Oruba, L., & Dormy, E. (2014). Transition between viscous dipolar and inertial multipolar dynamos. *Geophysical Research Letters*, *41*(20), 7115–7120. doi: 10.1002/2014GL062069

Panovska, S., Constable, C. G., & Korte, M. (2018). Extending global continuous geomagnetic field reconstructions on timescales beyond human civilization. *Geochemistry, Geophysics, Geosystems*, *19*(12), 4757–4772. doi: 10.1029/2018GC007966

Sanchez, S., Fournier, A., Aubert, J., Cosme, E., & Gallet, Y. (2016). Modelling the archaeomagnetic field under spatial constraints from dynamo simulations: a resolution analysis. *Geophysical Journal International*, *207*(2), 983–1002. doi: 10.1093/gji/ggw316

Schaeffer, N., Jault, D., Nataf, H.-C., & Fournier, A. (2017). Turbulent geodynamo simulations: a leap towards Earth's core. *Geophysical Journal International*, *211*(1), 1–29. doi: 10.1093/gji/ggx265

Sprain, C. J., Biggin, A. J., Davies, C. J., Bono, R. K., & Meduri, D. G. (2019). An assessment of long duration geodynamo simulations using new paleomagnetic modeling criteria (Q_{PM}). *Earth and Planetary Science Letters*, *526*, 115758. doi: 10.1016/j.epsl.2019.115758

Tauxe, L., & Kent, D. V. (2004). A simplified statistical model for the geomagnetic field and the detection of shallow bias in paleomagnetic inclinations: was the ancient magnetic field dipolar? In *Timescales of the paleomagnetic field* (pp. 101–115). American Geophysical Union (AGU). doi: 10.1029/145GM08

Thébault, E., Finlay, C. C., Beggan, C. D., Alken, P., Aubert, J., Barrois, O., ... Zvereva, T. (2015). International Geomagnetic Reference Field: the 12th generation. *Earth, Planets, and Space*, *67*, 79. doi: 10.1186/s40623-015-0228-9

Wardinski, I., & Korte, M. (2008). The evolution of the core-surface flow over the last seven thousands years. *Journal of Geophysical Research: Solid Earth*, *113*(B5). doi: 10.1029/2007JB005024

Wicht, J. (2002). Inner-core conductivity in numerical dynamo simulations. *Physics of the Earth and Planetary Interiors*, *132*(4), 281–302. doi: 10.1016/S0031-9201(02)00078-X

Wicht, J., & Meduri, D. G. (2016). A gaussian model for simulated geomagnetic field reversals. *Physics of the Earth and Planetary Interiors*, *259*, 45–60. doi: 10.1016/j.pepi.2016.07.007

Wicht, J., Stellmach, S., & Harder, H. (2015). Numerical dynamo simulations: From basic concepts to realistic models. In W. Freeden, M. Z. Nashed, & T. Sonar (Eds.), *Handbook of geomathematics* (pp. 779–834). Berlin, Heidelberg: Springer Berlin Heidelberg. doi: 10.1007/978-3-642-54551-1_16

Wicht, J., & Tilgner, A. (2010). Theory and modeling of planetary dynamos. *Space Science Reviews*, *152*(1), 501–542. doi: 10.1007/s11214-010-9638-y

Willis, A. P., Sreenivasan, B., & Gubbins, D. (2007). Thermal core-mantle interaction: Exploring regimes for "locked" dynamo action. *Physics of the Earth and Planetary Interiors*, *165*(1), 83–92. doi: 10.1016/j.pepi.2007.08.002

Yadav, R. K., Gastine, T., Christensen, U. R., Wolk, S. J., & Poppenhaeger, K. (2016). Approaching a realistic force balance in geodynamo simulations. *Proceedings of the National Academy of Sciences*, *113*(43), 12065–12070. doi: 10.1073/pnas.1608998113

References From the Supporting Information

Davies, C. J., Gubbins, D., & Jimack, P. K. (2011). Scalability of pseudospectral methods for geodynamo simulations. *Concurrency and Computation: Practice and Experience, 23*(1), 38–56. doi: 10.1002/cpe.1593

Ogg, J. G. (2012). In F. M. Gradstein, J. G. Ogg, M. D. Schmitz, & G. M. Ogg (Eds.), The geologic time scale (pp. 85–113). Elsevier, Boston. doi: 10.1016/B978-0-444-59425-9.00005-6

Pozzo, M., Davies, C., Gubbins, D., & Alfè, D. (2012). Thermal and electrical conductivity of iron at Earth's core conditions. *Nature, 485*, 355-358. doi: 10.1038/nature11031

Schaeffer, N. (2013). Efficient spherical harmonic transforms aimed at pseudospectral numerical simulations. *Geochemistry, Geophysics, Geosystems, 14*(3), 751–758. doi: 10.1002/ggge.20071